# Обзор ArXiv/astro-ph, 7-25 октября 2024

От Сильченко О.К.

# ArXiv: 2410.12091

## Globular cluster ages and their relation to high-redshift stellar cluster formation times from different globular cluster models

Lucas M. Valenzuela,[1]★ Duncan A. Forbes,[2] and Rhea-Silvia Remus[1]
[1]*Universitäts-Sternwarte, Fakultät für Physik, Ludwig-Maximilians-Universität München, Scheinerstr. 1, 81679 München, Germany*
[2]*Centre for Astrophysics & Supercomputing, Swinburne University, Hawthorn, VIC 3122, Australia*

Accepted XXX. Received YYY; in original form ZZZ

**ABSTRACT**

The formation details of globular clusters (GCs) are still poorly understood due to their old ages and the lack of detailed observations of their formation. A large variety of models for the formation and evolution of GCs have been created to improve our understanding of their origins, based on GC properties observed at $z = 0$. We present the first side-by-side comparison of six current GC formation models with respect to their predictions for the GC ages and formation redshifts in Milky Way (MW)-like galaxies. We find that all the models are capable of forming most of the surviving GCs at more than 10 Gyr ago, in general agreement with the observation that most GCs are old. However, the measured MW GC ages are still systematically older than those predicted in the galaxies of four of the models. Investigating the variation of modelled GC age distributions for general MW-mass galaxies, we find that some of the models predict that a significant fraction of MW-mass galaxies would entirely lack a GC population older than 10 Gyr, whereas others predict that all MW-mass galaxies have a significant fraction of old GCs. This will have to be further tested in upcoming surveys, as systems without old GCs in that mass range are currently not known. Finally, we show that the models predict different formation redshifts for the oldest surviving GCs, highlighting that models currently disagree about whether the recently observed young star clusters at high redshifts could be the progenitors of today's GCs.

**Key words:** globular clusters: general – galaxies: star clusters: general – Galaxy: formation – galaxies: formation

# Распределение реальных шаровых скоплений Галактики

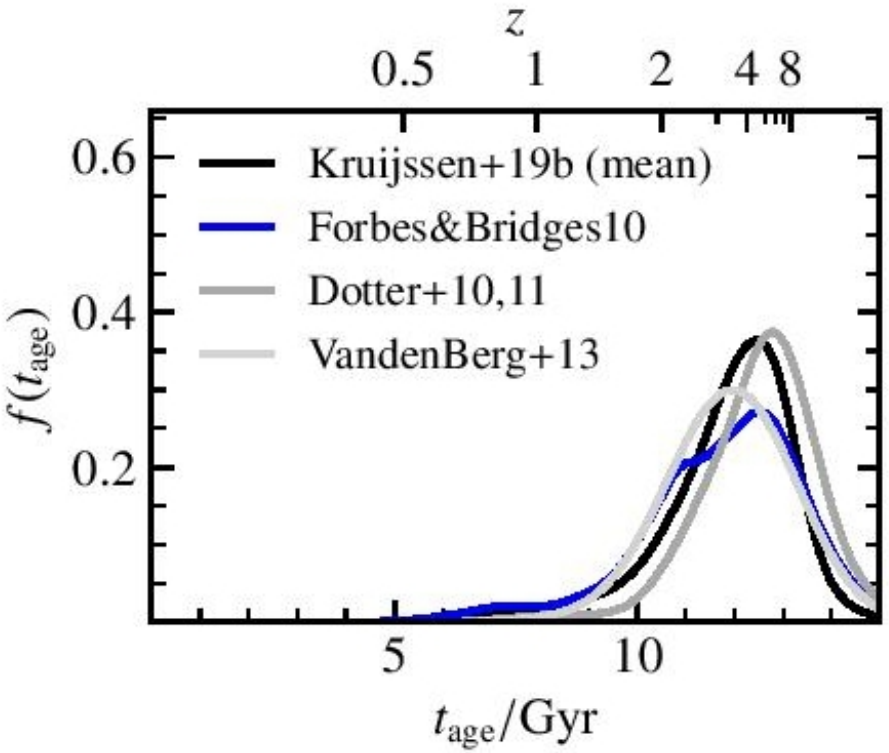


**Figure 1.** Age distributions of observed GCs in the MW. The ages are taken from Forbes & Bridges (2010), Dotter et al. (2010, 2011), VandenBerg et al. (2013), and Kruijssen et al. (2019b). The ages from the latter work are the mean ages from the other three studies, which we show as the black distribution. The smooth curves are determined from the sum of normal distributions at the individual age measurements with standard deviations equal to the individual age uncertainties.

# Модели

**Table 1.** Galaxy properties of the GC model studies and from the our MW: the number of MW-like galaxies analysed ($N_{gal}$), their virial and stellar mass ranges ($M_{vir}$ and $M_*$), the number of GCs contained in the individual galaxies ($N_{GC}$), the mean and standard deviation of $N_{GC}$, and the mean and standard deviation of the ages of all the GCs. The virial mass definitions are $M_{200}$ for Renaud et al. (2017), Kruijssen et al. (2019a), Reina-Campos et al. (2022), and Valenzuela et al. (2024); total mass of the system according to the applied subhalo finder for Chen & Gnedin (2024b); and halo mass for De Lucia et al. (2024). The GC-limited sample of De Lucia et al. (2024) is further selected according to $N_{GC}$. Note that the differences in GC number and average GC age are the result of the different galaxy samples. For the values measured from observations, the virial mass estimate is from Bobylev & Baykova (2023), which has also been proposed to be larger by other more recent works (e.g., Kravtsov & Winney 2024), the stellar mass from Licquia & Newman (2015), $N_{GC}$ from Garro et al. (2024), and we computed $\langle t_{age} \rangle$ using the mean GC ages from Kruijssen et al. (2019b).

| Model | Study | $N_{gal}$ | $M_{vir}/(10^{12}\,M_\odot)$ | $M_*/(10^{10}\,M_\odot)$ | $N_{GC}$ | $\langle N_{GC} \rangle$ | $\langle t_{age} \rangle$/Gyr |
|---|---|---|---|---|---|---|---|
| Stellar particle tracer | Renaud et al. (2017) | 1 | 1.3 | 4.1 (at $z = 0.5$) | – | – | $11.4 \pm 0.7$ |
| E-MOSAICS | Kruijssen et al. (2019a) | 6 | 0.7–2.2 | 0.8–4 | 60–330 | $130 \pm 100$ | $10.3 \pm 2.1$ |
| EMP-Pathfinder | Reina-Campos et al. (2022) | 21 | 0.6–2.3 | 0.4–6.5 | 140–1250 | $400 \pm 240$ | $8.1 \pm 3.5$ |
| Rapid mass growth | Chen & Gnedin (2024b) | 3 | 1.1–1.4 | 4–8 | 160–180 | $170 \pm 10$ | $11.2 \pm 1.4$ |
| Two-phase | De Lucia et al. (2024) | 12 884 | 0.8–3 | 2–8 | 0–11 100 | $290 \pm 590$ | $9.5 \pm 1.7$ |
| Two-phase (GC-limited) | De Lucia et al. (2024) | 1140 | 0.8–3 | 2–8 | 170–250 | $205 \pm 25$ | $10.8 \pm 1.1$ |
| Dual formation pathway | Valenzuela et al. (2024) | 21 | 1–2 | 1.6–4.4 | 220–700 | $400 \pm 120$ | $11.1 \pm 2.3$ |
| MW Observations | | – | $1.1 \pm 0.4$ | $6.1 \pm 1.1$ | $\gtrsim 200$ | – | $11.9 \pm 1.3$ |

# Распределение возрастов шаровых скоплений в моделях

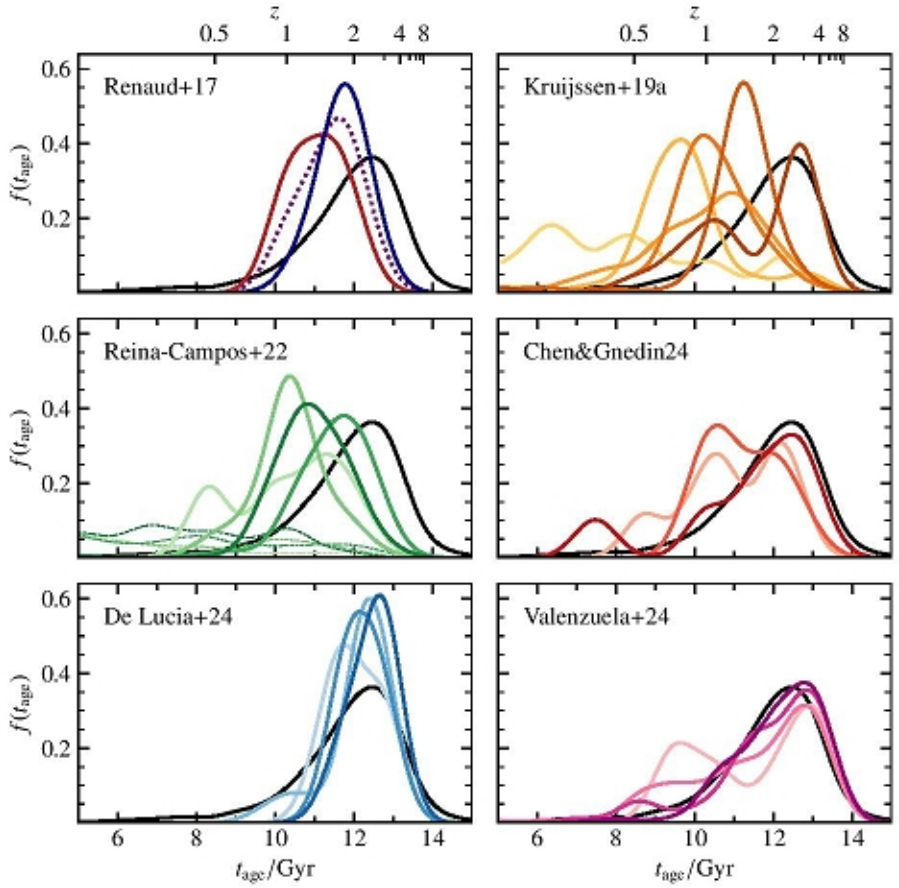


**Figure 2.** Age distributions of modelled GCs in MW-analogues compared to the observed GC ages in the MW. The full age distributions reaching to $t_{age} = 0$ Gyr are shown in Fig. A2. The observed GC ages are the mean values taken from Kruijssen et al. (2019b) and are shown in each panel as the black line. The modelled GC ages are from Renaud et al. (2017), Kruijssen et al. (2019a), Reina-Campos et al. (2022), Chen & Gnedin (2024b), De Lucia et al. (2024), and Valenzuela et al. (2024). The dotted blackberry line for Renaud et al. (2017) is the combined age distribution of the in-situ (red) and accreted (blue) GC age distributions, assuming an equal number of underlying GCs for each group. The dashed lines for Reina-Campos et al. (2022) correspond to the same galaxies as the solid distributions of equal colour, with the difference that no metallicity cut was applied to the GCs, which results in a large population of young star clusters. This is best seen in Fig. A2. The age distributions are determined from the sum of normal distributions at the individual age measurements with standard deviations equal to the individual age uncertainties. For the modelled GCs, we assume a uniform age uncertainty of 0.5 Gyr.

# Эпохи формирования шаровых скоплений в моделях

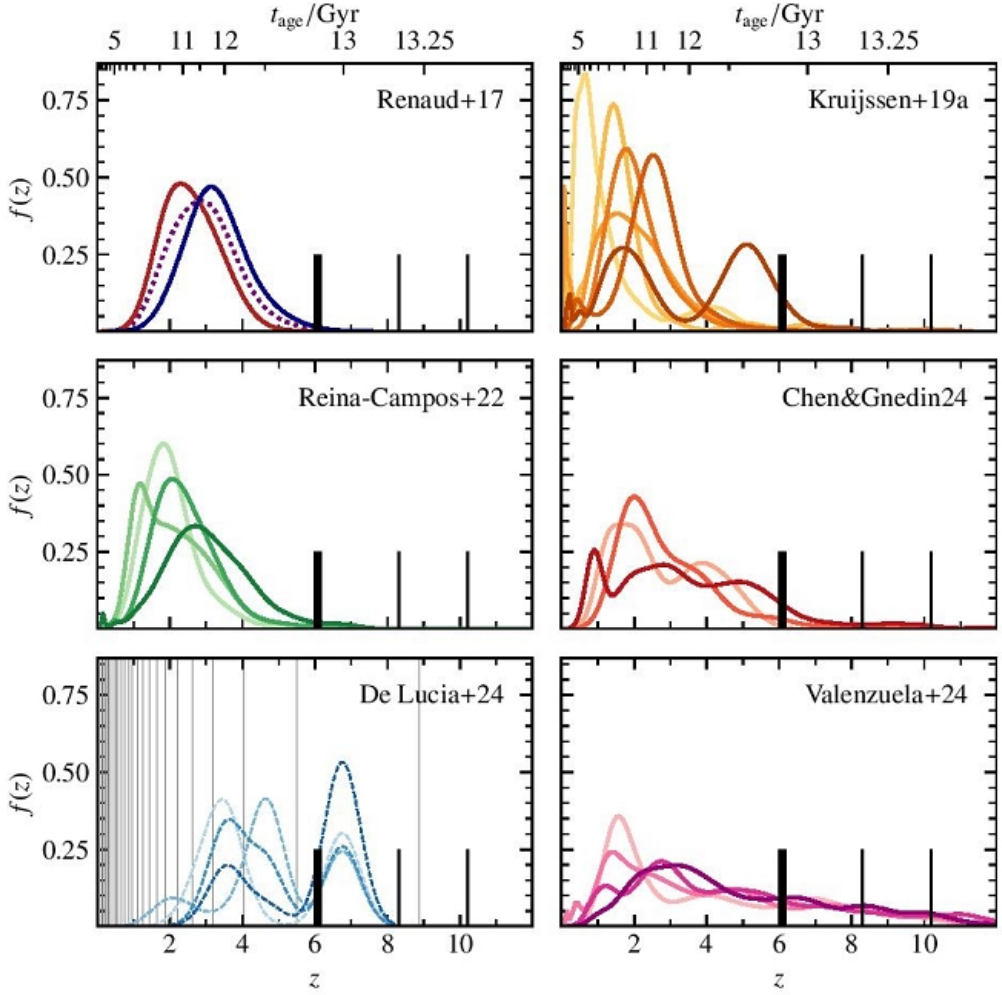


**Figure 4.** Formation redshift distributions of surviving modelled GCs in MW-analogues. The formation redshifts are from Renaud et al. (2017), Kruijssen et al. (2019a), Reina-Campos et al. (2022), Chen & Gnedin (2024b), De Lucia et al. (2024), and Valenzuela et al. (2024). The short vertical black lines denote the redshifts of star clusters from the strongly lensed systems observed by Vanzella et al. (2023), Fujimoto et al. (2024), Messa et al. (2024a), Mowla et al. (2024), and Adamo et al. (2024), in increasing redshift order. The dotted blackberry curve for Renaud et al. (2017) is the combined age distribution of the in-situ (red) and accreted (blue) GC age distributions, assuming an equal number of underlying GCs for each group. As the GC ages for the galaxies from De Lucia et al.

# Выводы

- Космологические модели НЕ предсказывают реальных шаровых скоплений
- Эмпирические модели формирования и эволюции галактик гораздо лучше – особенно модели автора

# ArXiv: 2410.17862

## The Most Massive Early-type Galaxies Exhibit Tidal Features More Frequently in Lower-density Environments

YONGMIN YOON [1], JAE-WOO KIM [1], AND JONGWAN KO [1,2]

[1] *Korea Astronomy and Space Science Institute (KASI), 776 Daedeokdae-ro, Yuseong-gu, Daejeon 34055, Republic of Korea*
[2] *University of Science and Technology, Gajeong-ro, Daejeon 34113, Republic of Korea*

ABSTRACT

The most massive early-type galaxies (ETGs) are known to form through numerous galaxy mergers. Thus, it is intriguing to study whether their formation in low-density environments, where nearby companions are almost absent, is associated with mergers, which are directly traced by tidal features. Using the 436 most massive ETGs with $M_{\rm star} > 10^{11.2}\,M_{\odot}$ at $z < 0.04$, we determine the variation in the fraction of massive ETGs with tidal features ($f_T$) across different environments and verify whether the most massive ETGs commonly have tidal features in very low density environments. Our main discovery is that the most massive ETGs exhibit tidal features more frequently in lower-density environments. In the highest-density environments, like galaxy clusters, $f_T$ is $0.21 \pm 0.06$, while in the lowest-density environments it triples to $0.62 \pm 0.06$. This trend is stronger for more extremely massive ETGs, with $f_T$ reaching $0.92 \pm 0.08$ in the lowest-density environments. One explanation for our finding is that the most massive ETGs in lower-density environments have genuinely experienced recent mergers more frequently than their counterparts in higher-density environments, suggesting that they possess extended formation histories that continue into the present. Another possibility is that tidal features last shorter in denser environments owing to external factors inherent in these environments. Our additional findings that massive ETGs with bluer $u-r$ colors are a more dominant driver of our main discovery and that dust lanes are more commonly observed in massive ETGs in low-density environments imply that gas-abundant mergers primarily contribute to the increased rate of recent mergers in low-density environments.

# Выборка ETG

- 0.01<z<0.04
- Log(M_*)>11.2
- NSA (NASA-Sloan Catalogue), DR11
- 659 → 436 массивных ETG
- Плотность окрестностей – среди 40515 галактик, log(M_*)>9.4

3. ENVIRONMENTS OF GALAXIES

In this study, we use two definitions to characterize the environments of galaxies. One is the surface number density of galaxies, calculated within the distance to the 10th-nearest galaxy, and another is the surface stellar mass density, determined using the 10 nearest neighboring galaxies. Both are calculated using NSA catalog galaxies with $\log(M_{\rm star}/M_{\odot}) \geq 9.4$ within a rest-frame velocity window of $\pm 1000$ km s$^{-1}$ centered on the redshift of each galaxy in the massive ETG sample.[4]

# Все галактики – красной последовательности

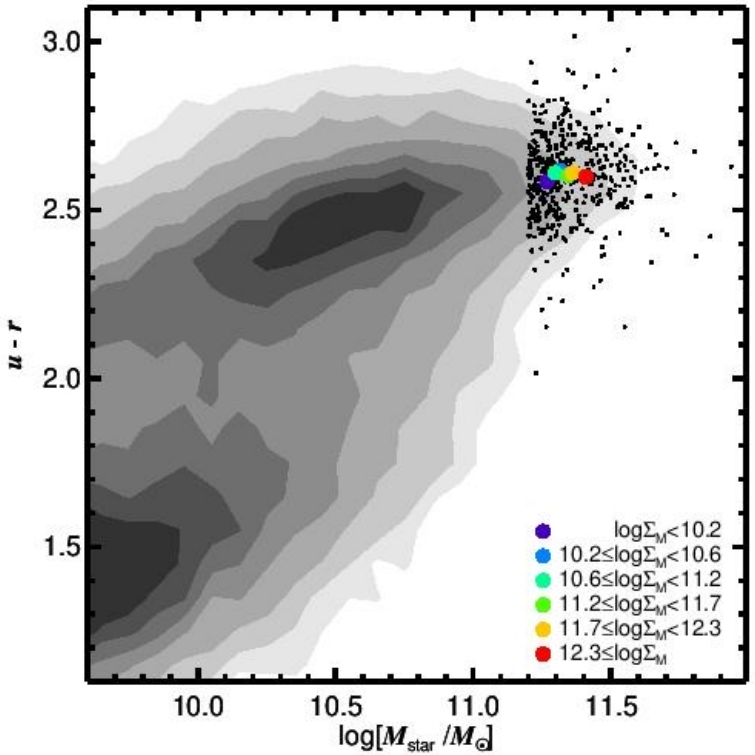


**Figure 7.** Diagram of $u - r$ color vs. stellar mass. The contours denote the density of all galaxies within $0.01 < z < 0.04$, with darker contours indicating higher densities. Massive ETGs with $\log(M_{\rm star}/M_\odot) > 11.2$ are plotted as black circles. We represent the median values of colors and stellar masses for massive ETGs in six different environments (quantified by $\log \Sigma_M$) using the circles of different colors. These six environment bins correspond to those used in Section 5. The units of $\Sigma_M$ are $M_\odot\,{\rm Mpc}^{-2}$.

# Результаты (по DESI, до 27й mag с кв. сек)

- Приливные структуры (хвосты, потоки, оболочки) – у 195, или 44.7% (для статистики оставлено 137).
- Пылевые прожилки – у 53 (12.2%).

# Галактики БЕЗ структур

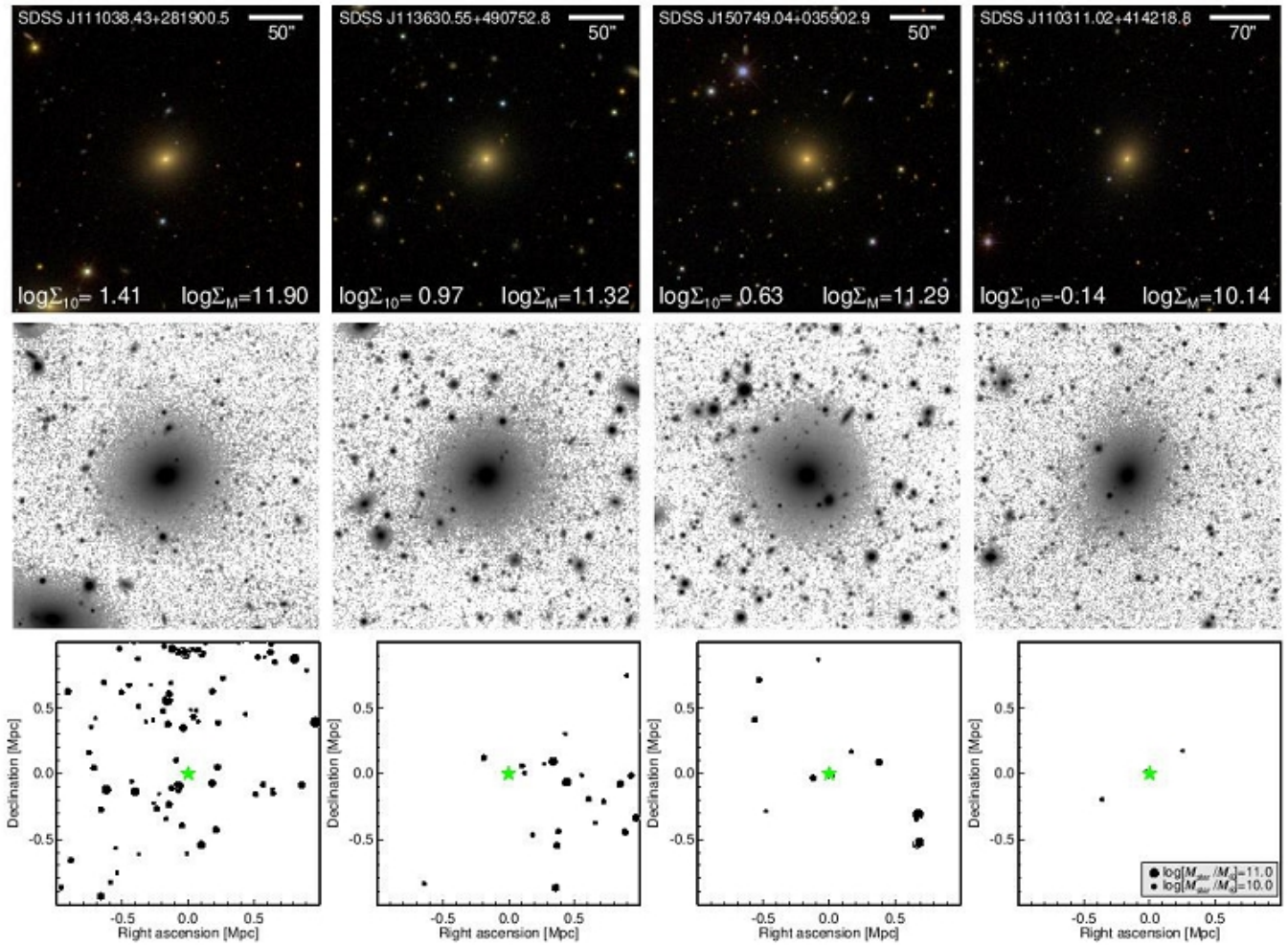


**Figure 1.** Examples of massive ETGs without tidal features. First row: color images from SDSS. The galaxy ID, $\log \Sigma_{10}$, and $\log \Sigma_M$ are displayed in the color images. The units of $\Sigma_{10}$ and $\Sigma_M$ are $\mathrm{Mpc}^{-2}$ and $M_\odot\,\mathrm{Mpc}^{-2}$, respectively. The horizontal bar in the color image denotes the angular scale of the image. Second row: $r$-band deep images of the DESI Legacy Survey. The angular scale of the deep image is identical to that of the color image in the first row. Third row: two-dimensional maps illustrating the spatial distribution of galaxies within $\sim 1$ Mpc from each massive ETG. The green star at the center of the map represents the location of the massive ETG, whereas the black filled circles denote other galaxies in the environment. The size of each circle indicates the galaxy's stellar mass, as shown in the legend in the bottom right panel. The ETGs are arranged such that the galaxy density decreases from the left to the right panels.

# Галактики с приливными структурами

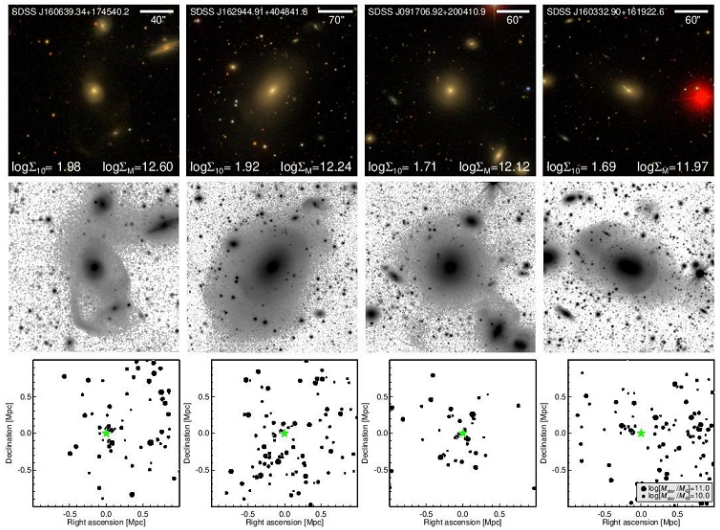


**Figure 2.** Examples of massive ETGs with tidal features, which are located in the environments with $\Sigma_{10} > 48$ (or $\log \Sigma_M > 11.9$), where the units of $\Sigma_{10}$ and $\Sigma_M$ are $\mathrm{Mpc}^{-2}$ and $M_\odot\,\mathrm{Mpc}^{-2}$, respectively. The other descriptions for this figure are the

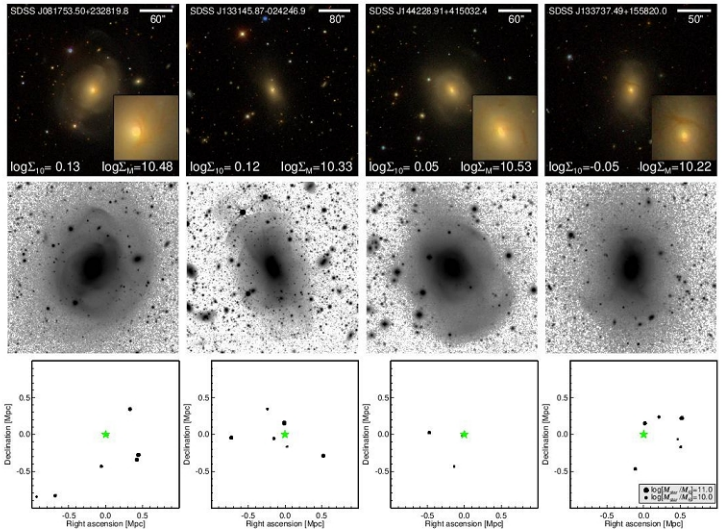


**Figure 4.** Examples of massive ETGs with tidal features, which are located in the environments with $0.8 < \Sigma_{10} < 1.4$ (or $10.2 < \log \Sigma_M < 10.6$), where the units of $\Sigma_{10}$ and $\Sigma_M$ are $\mathrm{Mpc}^{-2}$ and $M_\odot\,\mathrm{Mpc}^{-2}$, respectively. The inset images in the first row magnify the main body of each galaxy to clearly show the presence of dust lanes. The other descriptions for this figure are

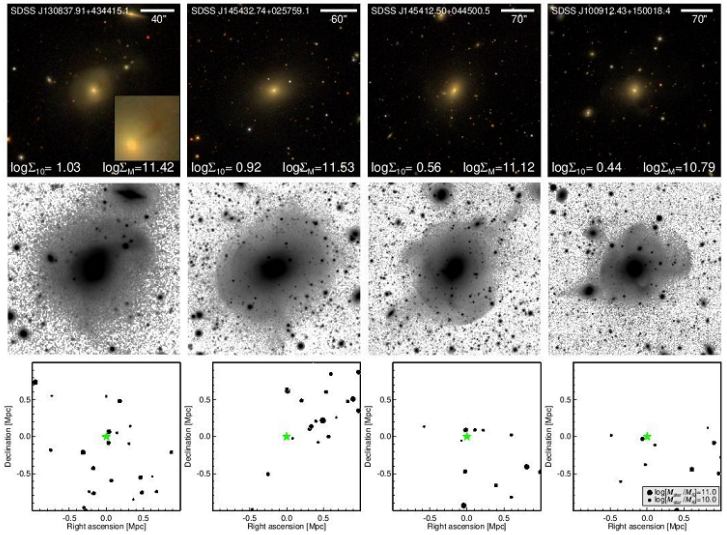


**Figure 3.** Examples of massive ETGs with tidal features, which are located in the environments with $2.7 < \Sigma_{10} < 11$ (or $10.7 < \log \Sigma_M < 11.6$), where the units of $\Sigma_{10}$ and $\Sigma_M$ are $\mathrm{Mpc}^{-2}$ and $M_\odot\,\mathrm{Mpc}^{-2}$, respectively. The inset in the first color image magnifies the main body of the galaxy to clearly show the presence of a dust lane. The other descriptions for this figure

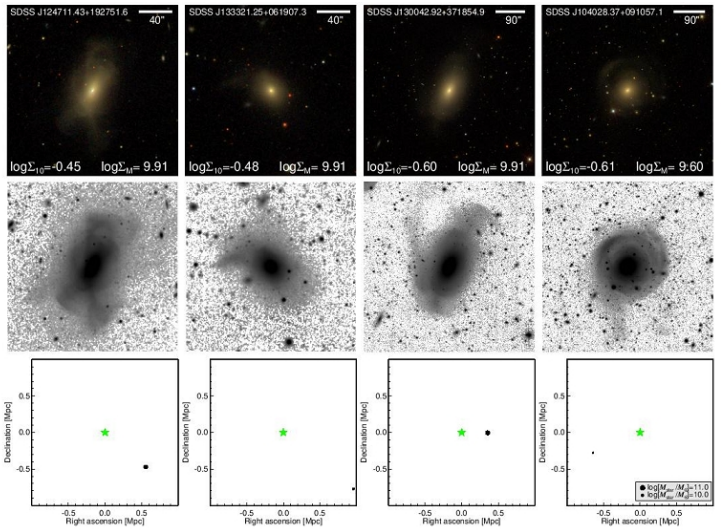


**Figure 5.** Examples of massive ETGs with tidal features, which are located in the environments with $\Sigma_{10} < 0.4$ (or $\log \Sigma_M < 10.0$), where the units of $\Sigma_{10}$ and $\Sigma_M$ are $\mathrm{Mpc}^{-2}$ and $M_\odot\,\mathrm{Mpc}^{-2}$, respectively. The other descriptions for this figure are the same as in Figure 1.

# Главный результат: следы мержинга – у галактик поля

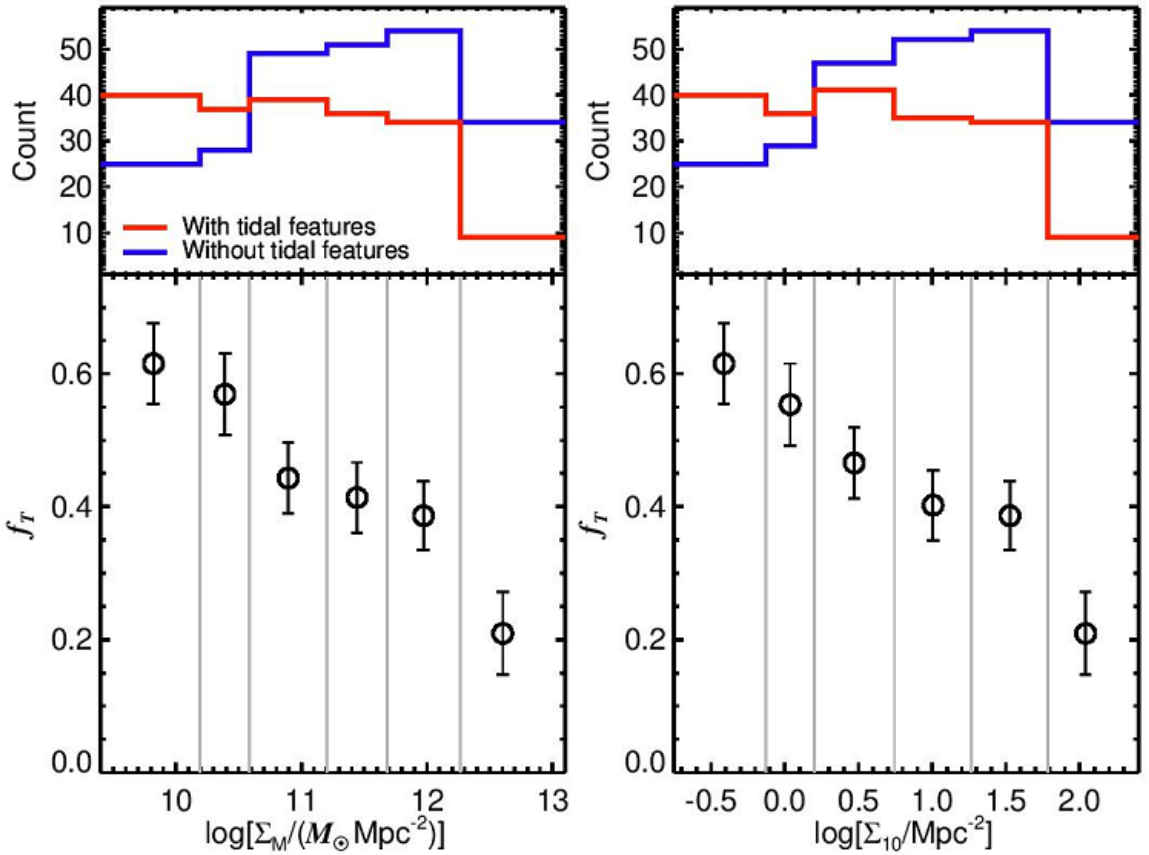


**Figure 8.** Fraction of massive ETGs with tidal features ($f_T$) as a function of $\log \Sigma_M$ (left panel) and $\log \Sigma_{10}$ (right panel). The fraction $f_T$ is calculated in six different environment bins corresponding to the percentile ranges of 0%–15%, 15%–30%, 30%–50%, 50%–70%, 70%–90%, and 90%–100% for both $\Sigma_M$ and $\Sigma_{10}$ of massive ETGs with $\log(M_{\rm star}/M_\odot) > 11.2$. The gray vertical lines represent the boundaries of the bins. The error bar indicates the standard error of the proportion. Displayed in the top panels are histograms of the distributions of $\log \Sigma_M$ and $\log \Sigma_{10}$ for ETGs with tidal features and those without tidal features.

The fraction $f_T$ is defined as $f_T = N_T/N_{\rm ETG}$, where $N_T$ statistical significance of the difference in the distribu-

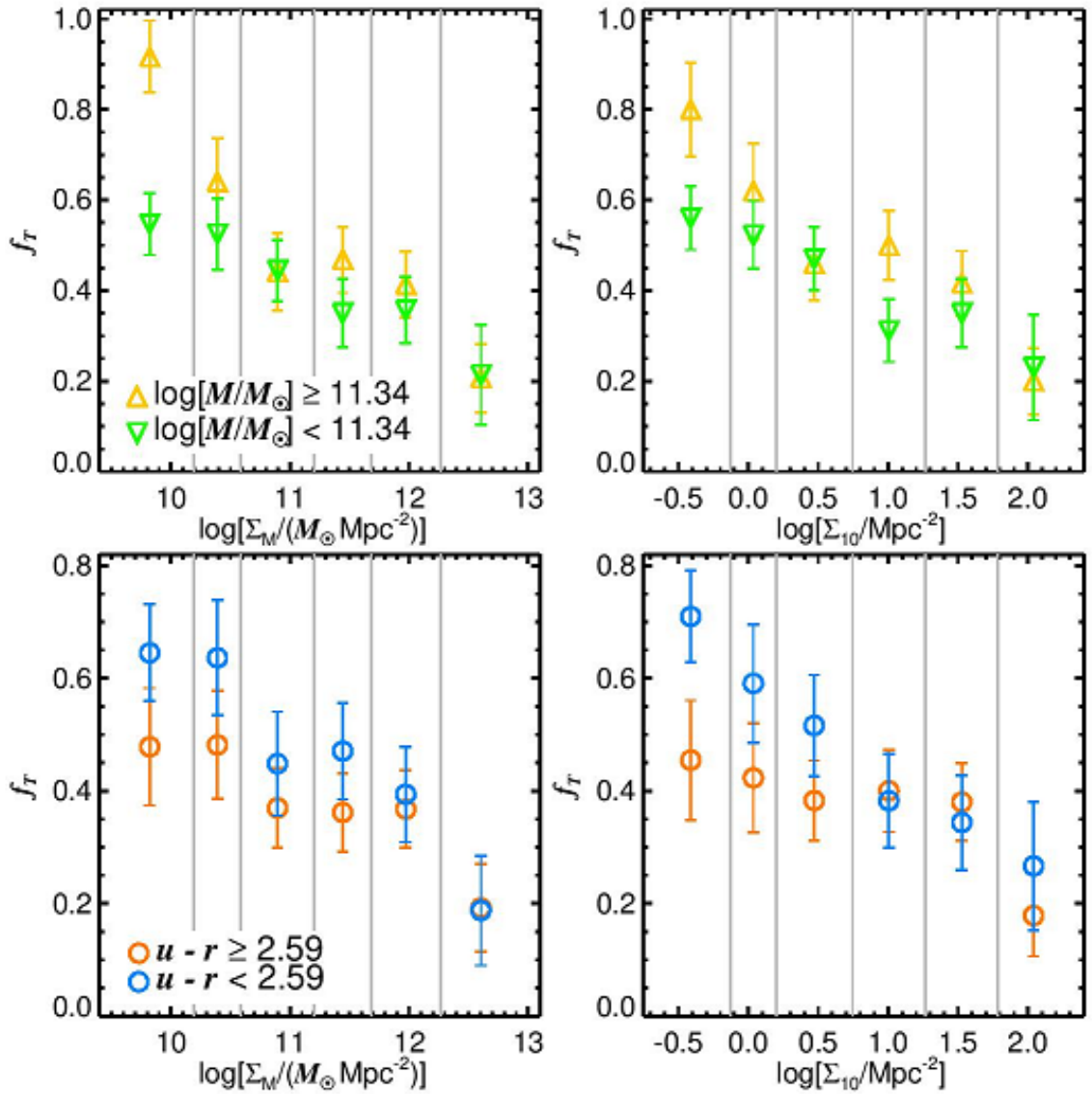


**Figure 9.** Top panels: fraction of massive ETGs with tidal features ($f_T$) as a function of $\log \Sigma_M$ and $\log \Sigma_{10}$ for two categories of massive ETGs, divided by a $\log(M_{\rm star}/M_\odot)$ threshold of 11.34, which approximately corresponds to the median $\log(M_{\rm star}/M_\odot)$ of the massive ETG sample. Bottom panels: $f_T$ as a function of $\log \Sigma_M$ and $\log \Sigma_{10}$ for two categories of massive ETGs, separated by a $u - r$ color threshold of 2.59, which is the average $u - r$ color of all the massive ETGs. In the bottom panels, we exclude ETGs with dust lanes that could significantly bias the color values. The fraction $f_T$ is calculated in the six different environment bins, as described in the caption of Figure 8. The gray vertical lines denote the boundaries of the bins. The error bar represents the standard error of the proportion.

# Похожая тенденция – у галактик с пылевыми прожилками

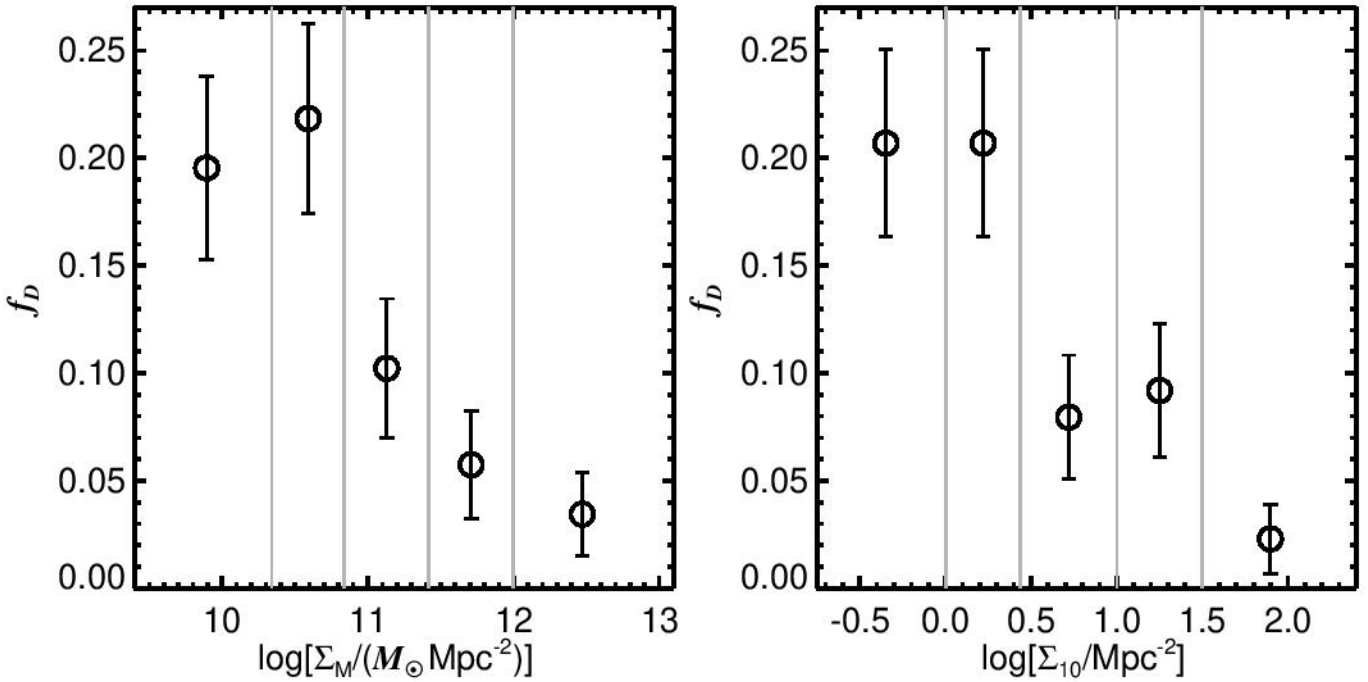


**Figure 10.** Fraction of massive ETGs with dust lanes ($f_D$) as a function of $\log \Sigma_M$ and $\log \Sigma_{10}$. The fraction $f_D$ is computed in five different environment bins corresponding to the percentile ranges of 0%–20%, 20%–40%, 40%–60%, 60%–80%, and 80%–100% for both $\Sigma_M$ and $\Sigma_{10}$ of massive ETGs with $\log(M_{\rm star}/M_\odot) > 11.2$. The gray vertical lines denote the boundaries of the bins. The error bar represents the standard error of the proportion.

# Два варианта интерпретаций:

- В плотном окружении (куда галактика попала недавно?) мержинг невозможен.
- Или наоборот, мержинг возможен, но его следы во внешних частях галактики быстрее рассасываются.